Estuarine, Coastal and Shelf Science 343 (2026) 110253

Contents lists available at ScienceDirect

Estuarine, Coastal and Shelf Science

journal homepage: www.elsevier.com/locate/ecss

Potential role of beach wrack in reducing storm overtopping on a Mediterranean urban beach: observations from Poetto Beach, Sardinia

Daniele Trogu [a,*], Antonio Usai [a], Simone Simeone [b], Marco Porta [a], Sandro Demuro [a]

[a] Department of Chemical and Geological Sciences, Coastal and Marine Geomorphology Group (CMGG), University of Cagliari, Monserrato, 09042, Italy
[b] CNR-IRBIM - Institute for Marine Biological Resources and Biotechnology - National Research Council, Oristano, 09170, Italy

ARTICLE INFO

Keywords:
Nature-Based solutions
Backshore inundation
Aeolian sediment trapping
Beach morphology
Coastal resilience
Posidonia oceanica

ABSTRACT

Beach wrack accumulations, composed of *Posidonia oceanica* remains and other vegetal debris, are common features along Mediterranean coasts but are frequently removed from beaches for aesthetic purposes. This study investigates the geomorphological and hydrodynamic role of beach wrack deposits in mitigating storm-wave overtopping and temporary backshore inundation events on a Mediterranean urban beach (Poetto beach, Sardinia, Italy). Two storm events characterised by comparable peak offshore wave heights, but different storm durations and backshore configurations, were investigated through an integrated approach combining coastal video monitoring, wave and wind reanalysis, hydrodynamic modelling, Total Water Level (TWL) analysis, DGPS-RTK surveys and infiltration measurements.

Despite a higher estimated TWL used as a first-order empirical indicator of storm-wave conditions, no berm overtopping or temporary backshore inundation was observed during the analysed recording interval when extensive mixed beach wrack deposits were present. In contrast, repeated berm overtopping and temporary backshore inundation occurred during the event characterised by the absence of beach wrack. Infiltration measurements showed that mixed wrack deposits exhibited higher permeability than the sandy backshore, while successive DGPS-RTK surveys documented post-storm aggradation associated with storm-wave redistribution and subsequent aeolian sediment trapping. Together, these processes promoted sediment retention and the progressive integration of beach wrack into the beach system.

These findings highlight the potential contribution of mixed beach wrack deposits to mitigating storm impacts and enhancing beach resilience. Rather than the natural deposits themselves, the potential Nature-Based Solution lies in adaptive management practices that preserve mixed wrack deposits *in situ* whenever compatible with local environmental and socio-economic conditions. Such management approaches may enhance the resilience of Mediterranean beaches to storm impacts and sea-level rise by supporting natural processes of wave energy dissipation, sediment retention and backshore accretion.

1. Introduction

Coastal zones are among the most dynamic and densely populated environments worldwide, hosting a large proportion of the global population and economic activities (Small and Nicholls, 2003; Nicholls and Cazenave, 2010; Neumann et al., 2015). In recent decades, increasing urbanisation and tourism development have significantly intensified anthropogenic pressure on coastal systems, particularly along Mediterranean shorelines where urban beaches represent key socio-economic assets (Barragán and De Andrés, 2015). At the same time, climate change is amplifying coastal hazards through sea-level rise and the increasing frequency and intensity of extreme storm events, enhancing the vulnerability of urban beaches to erosion and coastal flooding (Armaroli and Duo, 2018; Biondo et al., 2020; Vousdoukas et al., 2020; IPCC, 2023; Chatzipavlis et al., 2026). In this context, the adoption of sustainable coastal management strategies has become a priority for improving shoreline resilience and protecting both ecosystems and coastal infrastructure.

Among the different approaches proposed for coastal protection, Nature-Based Solutions (NBS) have gained increasing attention in recent years as sustainable strategies capable of reducing coastal risks while maintaining ecosystem functionality and biodiversity (Temmerman

* Corresponding author.
E-mail address: d.trogu@unica.it (D. Trogu).

https://doi.org/10.1016/j.ecss.2026.110253
Received 12 May 2026; Received in revised form 7 September 2026; Accepted 8 September 2026
Available online 8 September 2026

et al., 2013; European Commission, 2015; Narayan et al., 2016). These approaches rely on the capacity of natural ecosystems to regulate coastal processes such as wave attenuation, sediment retention and shoreline stabilisation. Coastal vegetated ecosystems, including seagrass meadows, are widely recognised for providing such ecosystem services while also contributing to climate regulation and carbon sequestration (Duarte, 2002; Ondiviela et al., 2014).

In Mediterranean coastal environments, one of the most relevant ecosystem components contributing to coastal stability is represented by seagrass ecosystems, particularly *Posidonia oceanica*. These meadows cover approximately 1–2% of the Mediterranean seabed and represent one of the most productive marine habitats in the region, playing a key role in biodiversity conservation, oxygen production and carbon sequestration (Mateo et al., 2003; Gobert et al., 2006; Telesca et al., 2015; Rotini et al., 2020).

Beyond their ecological importance in the marine environment, *Posidonia oceanica* also exerts a significant geomorphological influence on adjacent beaches. Detached seagrass leaves are commonly transported ashore by waves and currents, forming accumulations of organic material known as banquettes (Borum et al., 2004; Simeone and De Falco, 2012; Vacchi et al., 2017). These structures, often mixed with other vegetal debris such as driftwood, river reeds or woody remains, may accumulate along the backshore, forming thick organic berms commonly referred to as beach wrack (Boudouresque et al., 2016; Tomasello et al., 2022). Several studies have shown that these deposits can play a key role in coastal morphodynamics by dissipating wave energy, trapping sediments and increasing beach permeability (Kennedy and Woods, 2012; Ruju et al., 2022; Trogu et al., 2023).

Despite their recognised geomorphic and ecological functions, beach wrack deposits are frequently removed from beaches through mechanical cleaning operations, particularly in highly touristic areas (Simeone and De Falco, 2012). These practices are mainly driven by aesthetic considerations, as beach users often perceive banquettes as unpleasant or incompatible with recreational beach use. However, their removal can significantly alter beach morphology, reduce sediment retention and increase the vulnerability of coastal systems to storm impacts (Pikelj et al., 2022; Manfra et al., 2024).

Urban beaches represent a particularly critical context where the interaction between natural processes and human activities strongly influences coastal dynamics. While submerged *Posidonia oceanica* meadows provide a wide range of ecosystem services, including wave attenuation, sediment stabilisation and carbon sequestration, banquette and beach wrack deposits perform different geomorphological functions once accumulated on the shore. In such environments, mixed wrack deposits originating from both marine and terrestrial ecosystems can contribute to the formation of natural berms along the backshore, potentially acting as buffers against storm-wave overtopping and temporary backshore inundation. However, their role in these processes remains poorly studied, particularly on highly anthropised Mediterranean beaches.

In December 2019, exceptional rainfall events in southern Sardinia triggered intense fluvial transport of vegetal debris, mainly composed of *Arundo donax* reeds. Subsequent storm events transported and deposited large quantities of vegetal materials, together with *Posidonia oceanica* litter, along the urban beach of Poetto (Sardinia, Italy). The unexpected suspension of beach-cleaning activities during the COVID-19 lockdown allowed these deposits to remain undisturbed for several months, providing a unique opportunity to observe the natural morphodynamic evolution of vegetal accumulations in the absence of human interference (Ruju et al., 2022; Trogu et al., 2023). Within the monitored sector, the mixed beach wrack formed a continuous belt with an approximate cross-shore width of about 10 m. At the beach scale, the deposit extended along more than half of Poetto Beach, with the largest accumulations occurring in the south-eastern sector (Ruju et al., 2022; Trogu et al., 2023).

The present study investigates the geomorphological and hydrodynamic role of beach wrack deposits on Poetto beach by analysing two storm events characterised by comparable peak offshore significant wave heights and wave periods, but different wave direction, storm duration, integrated storm energy and antecedent morphology: one occurring in the absence of vegetal deposits and the other in the presence of abundant beach wrack material.

Specifically, this study aims to:

1. Analyse the influence of beach wrack deposits on wave overtopping processes and backshore inundation during storm events;
2. Evaluate the geomorphological response of the beach system under different backshore conditions;
3. Evaluate the management implications of mixed beach wrack deposits and discuss the potential of adaptive beach-wrack management as a Nature-Based Solution (NBS) for urban Mediterranean beaches.

To achieve these objectives, coastal video monitoring observations are integrated with DGPS-RTK topographic surveys, infiltration measurements, wave and wind datasets, Total Water Level estimates, storm-wave energy analysis and numerical hydrodynamic modelling, providing a comparative observational assessment of storm impacts on an urban Mediterranean beach.

It should be noted that the present analysis is based on the comparison of only two storm events and therefore does not aim to establish universally applicable relationships between beach wrack accumulations and storm-wave overtopping or backshore inundation processes. Rather, this study provides observational evidence from a representative Mediterranean urban beach, highlighting mechanisms that may influence backshore response under contrasting mixed beach wrack conditions. Previous studies have mainly focused on the geomorphological and hydrodynamic role of *Posidonia oceanica* banquettes, including their influence on swash dynamics and beach processes (Gómez-Pujol et al., 2013; Passarella, 2019). More recently, Ruju et al. (2022) investigated the geomorphological and hydraulic behaviour of mixed beach wrack deposits composed of *P. oceanica* remains and terrestrial vegetal debris. Building on these studies, the present work extends previous research by examining how the presence of an extensive mixed wrack deposit relates to contrasting beach responses observed during two real storm events. The combined analysis of wave uprush and backshore inundation, beach morphology, and infiltration provides further observational evidence of the potential role of mixed beach wrack in influencing backshore response under storm conditions. Although site-specific, these findings provide a useful basis for future investigations involving a larger number of storm events and different coastal settings, thereby contributing to a broader understanding of the potential role of beach wrack deposits in enhancing coastal resilience.

2. Study area

Poetto beach is located along the southern coast of Sardinia Island (western Mediterranean Sea), within the Gulf of Cagliari (Italy) (Fig. 1a). The beach extends for approximately 8 km alongshore and reaches a maximum cross-shore extension of about 100 m (Fig. 1). Geomorphologically, the coastal system is bounded to the west by the S. Elia Promontory, which separates Poetto beach from the Giorgino beach system located on the western side of the promontory (Porta et al., 2020).

Poetto is a microtidal, wave-dominated urban sandy beach characterised by a predominantly south-eastern wave exposure due to the geographic orientation of the Gulf of Cagliari (De Muro et al., 2017; Trogu et al., 2023). Tidal excursions are generally lower than 0.2 m, reaching approximately 0.4 m during spring tides (Brambilla et al., 2016; Trogu et al., 2023; ISPRA, 2026), and coastal dynamics are mainly controlled by wave forcing and storm events generated within the western Mediterranean basin. The nearshore area is characterised by

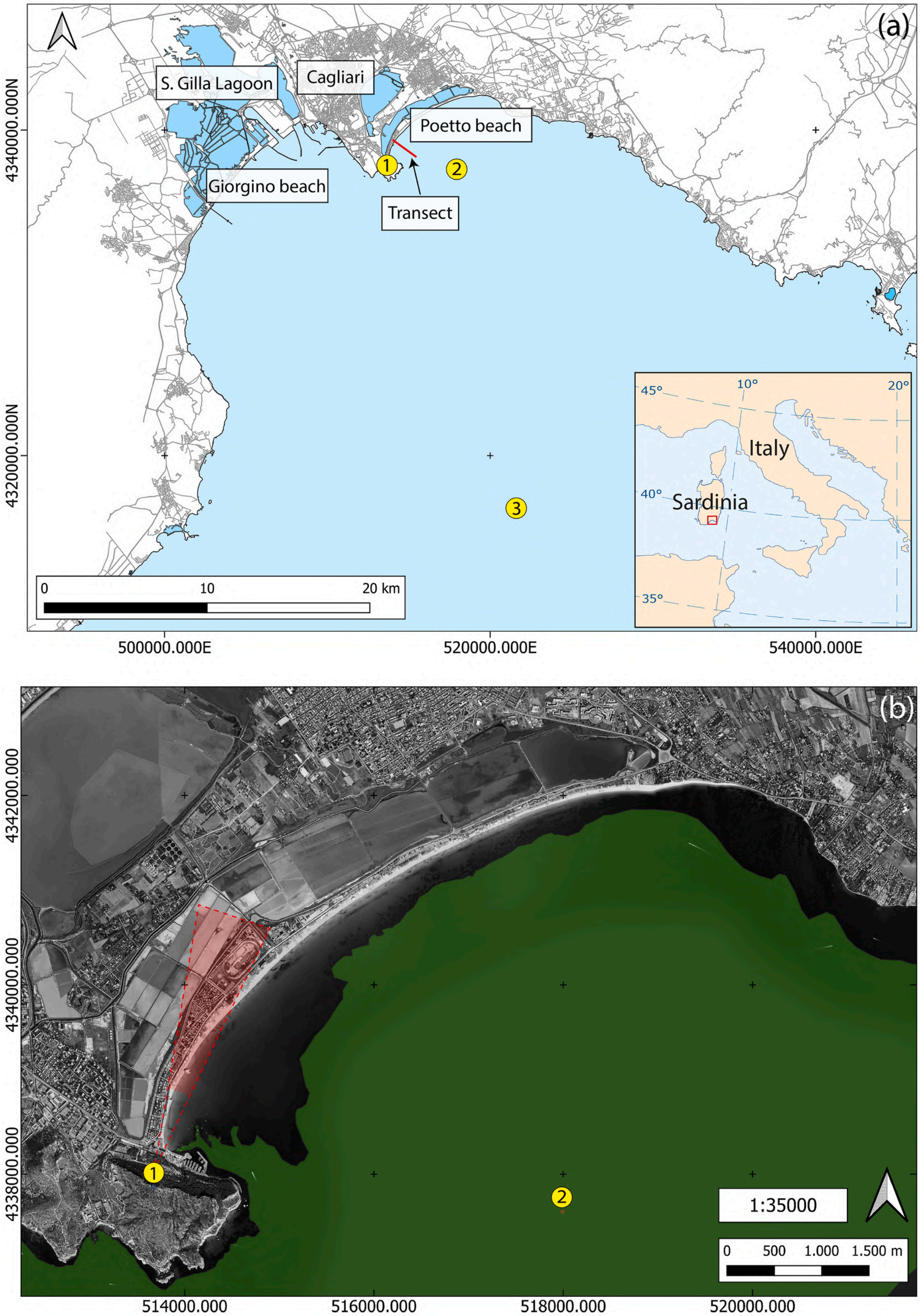

Fig. 1. Location of the study area: the upper panel **(a)** shows an overview of the Gulf of Cagliari. The lower panel **(b)** presents a detailed view of Poetto beach, including the area covered by the coastal video monitoring system (red box), and the distribution of the *Posidonia oceanica* meadow (green area). The yellow dots indicate: (1) camera position; (2) Copernicus Marine Environment Monitoring Service (CMEMS) grid node; (3) ERA5 grid node. Coordinate system: UTM 32N; datum: WGS84. (For interpretation of the references to colour in this figure legend, the reader is referred to the Web version of this article.)

the presence of an extensive *Posidonia oceanica* meadow (green area in Fig. 1b), which represents the main source of biogenic sediments supplying the beach system (De Muro et al., 2017; Porta et al., 2020). The backshore, beachface and nearshore sediments of Poetto Beach are predominantly composed of mixed siliciclastic–bioclastic sands. The backshore and beachface are characterised by a dominant siliciclastic fraction (approximately 75%) associated with a significant bioclastic component (approximately 20%), while the bioclastic contribution increases seawards in relation to the presence of *Posidonia oceanica* meadows. Since 2002, the carbonate fraction of the beach sediments has increased as a result of a nourishment intervention carried out in the southwestern sector of Poetto Beach. The nourishment involved the placement of bioclastic sediments, characterised by a grain size different from that of the native beach material, using a dredger. The nourished sediments were subsequently redistributed and levelled along the beach using bulldozers (Trogu et al., 2023).

Unlike many Mediterranean coastal systems, Poetto beach is not directly intersected by rivers. However, several fluvial systems draining the Campidano and Cixerri plains discharge into the nearby Santa Gilla Lagoon, which is hydraulically connected to the Gulf of Cagliari (Porta et al., 2020; Ruju et al., 2022). During intense rainfall events, these river systems can transport large quantities of vegetal debris toward the coastal zone, contributing to the supply of organic material that may subsequently be redistributed along the shoreline by waves and coastal currents (Ruju et al., 2022).

The study focuses on the western sector of Poetto beach, which is monitored by a coastal video monitoring station installed on the S. Elia Promontory (Fig. 1). The station, located approximately 125 m above sea level, overlooks the western portion of the beach and provides continuous observations of nearshore processes across the surf zone and the backshore. This sector was selected as the main observation area for the detailed analysis presented in this study because it is the portion of Poetto Beach best covered by the coastal video monitoring system and is supported by complementary DGPS-RTK surveys and infiltration measurements.

Poetto beach represents one of the most important urban beaches in Sardinia and is subjected to intense anthropogenic pressure associated with tourism, recreational activities and urban development. During the spring and summer seasons, beach-cleaning operations are routinely performed using heavy machinery to remove vegetal debris and seagrass deposits from the backshore, primarily to enhance beach aesthetics and usability. (Porta et al., 2020). However, these practices may significantly alter the natural morphodynamic behaviour of the beach system, potentially reducing its resilience to storm impacts (Brambilla et al., 2016; Biondo et al., 2020).

3. Materials and methods

3.1. Coastal video monitoring and image processing

The storm events analysed in this study were investigated using imagery acquired from the coastal video monitoring system operated by the Coastal and Marine Geomorphology Group (University of Cagliari). The coastal monitoring station is installed on the S. Elia Promontory at approximately 125 m above sea level and provides a panoramic view of the western sector of Poetto beach.

The coastal video monitoring system consists of a fixed digital camera acquiring image sequences (*snapshots*) four times per day. Each acquisition consists of a video sequence recorded at 4 Hz, producing high-resolution images (4096 × 2160 pixels) suitable for analysing nearshore hydrodynamic processes. The image processing and analysis procedures were implemented using custom MATLAB scripts, including image calibration, rectification, georeferencing and generation of time-stack images. Lens-induced distortions were corrected using camera calibration parameters including focal length, principal point position and radial and tangential distortion coefficients (Passarella, 2019).

After calibration, the images were rectified and georeferenced using twelve Ground Control Points (GCPs) identified on the imagery and orthophotos from the WMS of the "Regione Autonoma della Sardegna" (Sardegna Geoportale, 2026). The twelve GCPs were distributed across the monitored sector, with a higher density in the portion of the image encompassing the analysed cross-shore transect, where the highest geometric accuracy was required. Image coordinates were transformed into real-world coordinates using the WGS84–UTM 32N reference system following Trogu et al. (2023). The resulting plan-view images were generated on a 0.15 × 0.15 m grid, with root mean squared georeferencing errors of 0.13 m and 0.38 m in the easting ($RMSE_E$) and northing ($RMSE_N$) directions, respectively (Passarella, 2019). Time-stack images were generated along a cross-shore transect shown in Fig. 2 to analyse swash dynamics during the selected storm events. Swash fronts were manually digitised from the georeferenced time-stack images, and the maximum landward extent of each wave uprush event was subsequently identified along the analysed transect. The maximum swash extent was defined as the furthest landward position reached by the visible uprush along the analysed transect. Under inundated backshore conditions, the advancing swash front was identified by tracking the characteristic texture and brightness contrast of the moving wave front relative to the surrounding standing water. The same interpretation criteria were consistently applied to all analysed time-stack images by the same operator. This image analysis provides the maximum observed landward excursion of wave uprush during the analysed recording intervals rather than a quantitative assessment of overtopping frequency or overtopping discharge.

Two storm events were analysed: 29 October 2018 and 21 January 2020 (Fig. 2). For each event, representative time intervals were selected to generate time-stack images and compare the swash behaviour and wave overtopping processes under different backshore conditions.

3.2. Topographic surveys and infiltration tests

Cross-shore beach profiles were surveyed using a Differential Global Positioning System (DGPS) operating in Real Time Kinematic (RTK) mode, consisting of a GNSS receiver (NavCom SF-3040, StarFire) connected in real time to the NETGEO correction network. The system provided a horizontal accuracy of 1 cm + 0.5 ppm and a vertical accuracy of 2 cm + 1 ppm.

Beach topography was acquired along predefined cross-shore transects extending from the backshore to the shoreline. During the surveys, the GNSS antenna was mounted on a levelling rod to minimise operator-induced errors, particularly in the vertical component. Position data were acquired at a frequency of 1 Hz, and, for each surveyed point, ten consecutive XYZ measurements were acquired to improve positional accuracy.

All coordinates were referenced to the WGS84–UTM Zone 32N coordinate system. The surveys were conducted shortly before each analysed storm event, specifically 10 days prior to the 2018 event and one day before the 2020 event. Given the absence of significant hydrodynamic forcing between the survey dates and the onset of the storms, the acquired profiles were considered representative of the pre-storm foreshore morphology. An additional DGPS-RTK survey was carried out approximately three months after the January 2020 storm to assess the post-storm morphological evolution associated with aeolian sediment transport during the COVID-19 lockdown period, when beach-cleaning activities were suspended. The DGPS-RTK profiles were subsequently used to characterise beach morphology, identify the position and elevation of the berm crest, and estimate the foreshore slope ($\tan \beta_f$), calculated as the ratio between the elevation difference and the horizontal distance between mean sea level ($z = 0$) and the berm crest.

Infiltration measurements were conducted along a transect located a few meters from the study transect to characterise the hydraulic properties of the different beach environments and beach wrack deposits. Tests were performed at selected locations on the backshore, swash zone and mixed wrack ridge composed of buried *Arundo donax* reeds and *Posidonia oceanica* remains using double-ring infiltrometers following ASTM D3385. Due to the extremely high infiltration capacity of a nearby *Posidonia oceanica* banquette, additional measurements were performed using a simplified single-ring infiltrometer. A subset of these measurements was previously presented by Ruju et al. (2022).

3.3. Wave and wind data

Wave conditions during the analysed storm events were obtained

Fig. 2. Snapshots acquired from the coastal video monitoring system during the two analysed storm events: **(a)** 29 October 2018; **(b)** 21 January 2020. The red dashed line indicates the location of the cross-shore transect used for the extraction of time-stack images. (For interpretation of the references to colour in this figure legend, the reader is referred to the Web version of this article.)

from the Copernicus Marine Environment Monitoring Service – CMEMS (Product ID: MEDSEA_MULTIYEAR_WAV_006_012; Korres et al., 2021) using data extracted from a hindcast located in a grid node of the model, offshore of Poetto beach in the Gulf of Cagliari, located at 39°11′15″ N, 9°12′30″ E (Fig. 1). The hindcast dataset covers the period from 1 January 1985 to 30 April 2026 and provides hourly values of significant wave height (H_s), peak wave period (T_p), mean wave period (T_m) and mean wave direction (*Dir*). The suitability of this CMEMS hindcast for representing wave conditions at Poetto Beach has previously been validated by Chatzipavlis et al. (2026), and the extracted wave parameters were used to characterise the hydrodynamic conditions associated with the selected storm events. Wave directions are expressed as the direction from which the waves originate, following the nautical convention (0° = geographic north, clockwise positive).

For the two storm events analysed in this study, a Peak Over Threshold (POT) approach (Mathiesen et al., 1994) was applied to the wave time series in order to identify and characterise the storm conditions. Sea states were classified as storm conditions when the significant wave height (H_s) exceeded the 99.5 percentile for at least 12 consecutive hours. To avoid double counting, peaks occurring within 48 h were considered part of the same event. This procedure allowed the identification of the temporal extent of each storm and the computation of storm duration. For each event, a total storm wave energy index (E^i_{tot}) was computed over the duration of the storm, following the formulation proposed by Molina et al. (2019):

$$E^i_{tot} = \int_0^{d_i} \frac{\rho g^2}{64\pi} T_e H_s^2 dt \quad [1]$$

where d_i is the duration of the storm, ρ is water density, g is the gravity acceleration, T_e is the energy period, estimated from the peak wave period as $T_e = 0.9\ T_p$, consistent with the typical approximation for a JONSWAP spectrum, H_s is the significant wave height (m), and dt is the temporal resolution of the dataset (1 h). This index represents a discrete approximation of the time-integrated wave energy associated with each storm event and was used to quantify their relative intensity, consistent with the physical dependence of wave energy on wave height and period (Komar, 1998; Holthuijsen, 2007). Accordingly, the use of offshore H_s and T_p provides only a first-order approximation of the hydrodynamic forcing at the study site.

To provide a first-order estimate of the potential for wave-driven backshore inundation during the analysed storm events, the Total Water Level (TWL) was calculated for the camera recording interval following the formulation proposed by Pugh (1987):

$$TWL = Z_0(t) + T(t) + R(t) \quad [2]$$

where $Z_0(t)$ is the non-tidal residual water level, including storm surge effects; $T(t)$ is the astronomical tidal component; and $R(t)$ is the wave runup component.

Time series of $Z_0(t)$ and $T(t)$ were derived from the tide gauge records of the Port of Cagliari, operated within the Italian National Tide Gauge Network (ISPRA, 2020). The wave runup component ($R_{2\%}$) was estimated using the empirical formulation proposed by Stockdon et al., which predicts the 2% exceedance wave runup. The foreshore slope ($\tan \beta_f$) was derived from the DGPS-RTK beach profiles acquired prior to each storm event. Offshore significant wave height (H_0) was approximated using the significant wave height (H_s) obtained from CMEMS wave data, whereas the deep-water wavelength (L_0) was estimated from the peak wave period (T_p) following the linear wave theory (Airy, 1845) as:

$$L_0 = \frac{gT_p^2}{2\pi} \quad [3]$$

where g is the gravity acceleration and T_p is the peak period.

The estimated TWL values were used as a first-order indicator of the relative potential for wave overtopping and temporary backshore inundation during the two analysed storm events.

Wind conditions were obtained from the ERA5 reanalysis dataset (Hersbach et al., 2023). Hourly wind speed at 10 m above sea level (U_{10}) and wind direction (Dir_w) were extracted from the ERA5 grid node closest to the study area (product ID: reanalysis-era5-single-levels), located at 39°00′00″ N, 9°15′00″ E (Fig. 1). Although its spatial resolution does not resolve local coastal wind variability, ERA5 has been shown to reproduce the general temporal variability of surface winds in Mediterranean coastal regions and was therefore used to characterise the synoptic wind conditions associated with the analysed storm events (Patra et al., 2025). Wind directions are reported as coming from the indicated direction, following the nautical convention (0° = geographic north).

3.4. Hydrodynamic modelling

To provide a general overview of the hydrodynamic circulation in the Gulf of Cagliari during the two storm events and to describe only the broader hydrodynamic context, two simulations were performed using the Delft3D modelling (Deltares) (software version: 4.04.01) coupling the FLOW (Lesser et al., 2004) and WAVE (Booij et al., 1999; Ris et al., 1999) modules (see supplementary materials Table SM 1). The simulations were intended solely to illustrate the circulation patterns within the Gulf of Cagliari and were not used to investigate the flood-mitigation mechanism associated with beach wrack deposits. Although the model

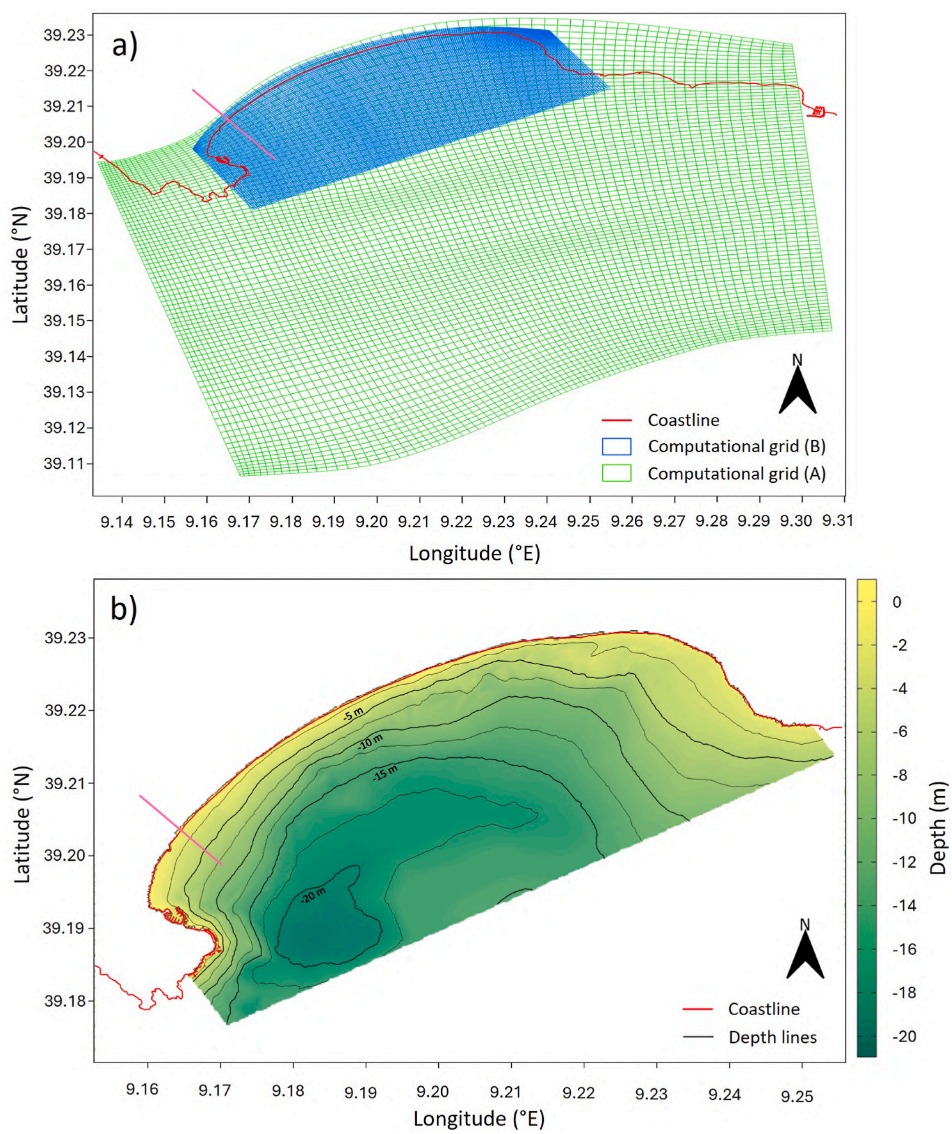

Fig. 3. Hydrodynamic modelling setup: (a) nested computational grids used for the coupled hydrodynamic wave model, with grid A (green) covering the Gulf of Cagliari and grid B (blue) providing higher-resolution simulations for the Poetto beach area; (b) bathymetry used for grid B to simulate nearshore hydrodynamic circulation. Pink lines indicate the location of the cross-shore transects used for the analysis. (For interpretation of the references to colour in this figure legend, the reader is referred to the Web version of this article.)

was not specifically validated for the analysed storm events, the simulated circulation patterns were consistent with those previously reported for the Gulf of Cagliari by Brambilla et al. (2016) and by Ruju et al. (2019, 2022).

The WAVE module (based on the SWAN model) was used to simulate wave propagation from offshore toward the nearshore zone, while the FLOW module was used to compute depth-averaged hydrodynamic circulation patterns. Two computational grids with different spatial resolutions were implemented (Fig. 3). A larger grid (Grid A; mean cell size: 150 × 125 m), covering the Gulf of Cagliari, was used to propagate offshore wave conditions toward the coastal zone, while a finer nested grid (Grid B; mean cell size: 30 × 30 m) was applied to simulate nearshore hydrodynamics along Poetto beach (Fig. 3a, supplementary materials Table SM 2). The bathymetric dataset used in the model was derived from a combination of nearshore bathymetric surveys and the EMODnet digital bathymetric model (EMODnet Bathymetry Consortium, 2024). The bathymetry used for the larger grid (Grid A) ranges from 0 m to −70 m, whereas the bathymetry adopted for the finer grid (Grid B) ranges from 0 m to −25 m (Fig. 3b–Table SM 2). The simulations were performed using the default physical parameter settings provided by the Delft3D software for both the FLOW and WAVE modules (e.g. depth-induced wave breaking, seabed roughness, etc.). Consequently, processes such as sediment transport and bottom friction induced by the presence of *Posidonia oceanica* meadows were not explicitly considered in the modelling framework (Table SM2).

Wave parameters (H_s, T_p and Dir) and wind data (U_{10} and Dir_w) (see supplementary materials Table SM 1) were applied at the offshore domain boundaries (uniform boundary conditions with directional spreading = 4 cosine power). Each simulation covered a 72-h time window (Computational Mode: No-Stationary; Time steps: 60 s), selected to include pre-storm conditions, the peak phase of each event, and the time interval corresponding to the video monitoring observations, allowing the reconstruction of the key hydrodynamic processes associated with each storm event (Table SM 1).

4. Results

4.1. Storm event characteristics

Two storm events affecting Poetto beach were analysed: 29 October 2018 and 21 January 2020 (Table 1; Fig. 4). Wave data derived from CMEMS indicate that both events were characterised by comparable peak offshore wave heights and wave periods, while differing in mean wave direction, storm duration, and integrated wave energy. A Peak-Over-Threshold (POT) analysis performed on the complete CMEMS hindcast dataset (1 January 1985–30 April 2026) identified a 99.5th percentile threshold of 1.85 m for significant wave height (H_s), which was subsequently used to identify extreme storm events. Both analysed storms exceeded this threshold. During the October 2018 storm event, the daily average significant wave height (H_s) reached 2.2 m, with peak values of 2.9 m (Table 1). The corresponding peak wave period (T_p) reached values of 9.2 s. Similarly, during the January 2020 event, the daily average significant wave height (H_s) was 2.7 m, with peak values also reaching 2.9 m, while the peak wave period (T_p) reached the same maximum value of 9.2 s (Table 1). The mean wave direction (Dir) during both events was predominantly from the southern to south-eastern sectors (Table 1; Fig. 4), reflecting the main storm wave approach typical of the Gulf of Cagliari (Usai et al., 2025a, 2025b). For all these reasons, the two storm events provided an opportunity to investigate the influence of contrasting backshore configurations, particularly the presence or absence of mixed beach wrack deposits, during storms characterised by comparable peak offshore significant wave heights and wave periods.

Table 1
Wave parameters (significant wave height, H_s; peak wave period, T_p; mean wave period, T_m; wave direction, Dir) for the two analysed storm events (29 October 2018 and 21 January 2020), including daily average values, daily peak values and values corresponding to the camera recording interval.

Wave parameter	29 October 2018			21 January 2020		
	Daily average value	Daily peak value	Value during camera interval	Daily average value	Daily peak value	Value during camera interval
H_s (m)	2.2	2.9	2.5	2.7	2.9	2.6
T_p (s)	8.9	9.2	9.2	8.5	9.2	9.2
T_m (s)	5.3	6.4	5.0	6.0	6.2	6.1
Dir (°)	167	147	184	137	138	138

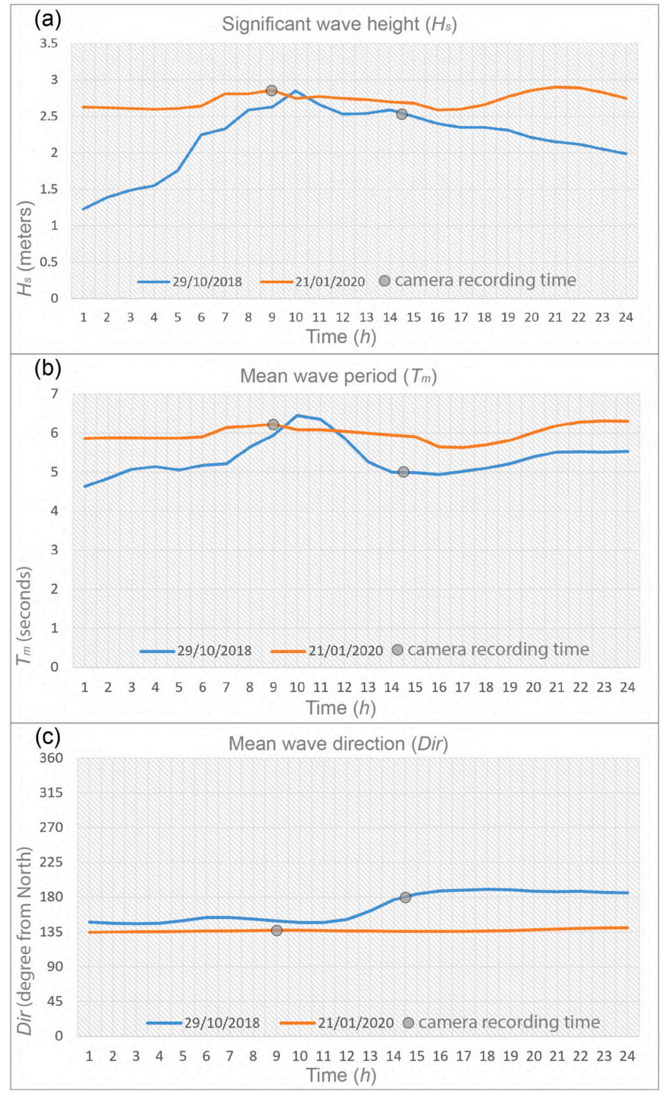

Fig. 4. Wave conditions derived from the CMEMS hindcast dataset during the two storm events analysed (29 October 2018 and 21 January 2020): **(a)** significant wave height (H_s), **(b)** mean wave period (T_m) and **(c)** wave direction (Dir). The grey dot indicates the time corresponding to the camera recording interval.

Wind conditions during the two storm events showed comparable intensities (U_{10}) but different directions (Dir_w) (Table 2; Fig. 5). During the 29 October 2018 storm event, wind speeds (U_{10}) reached a daily average of 12.0 m s^{-1}, with peak values of 15.2 m s^{-1} and values of about 14.0 m s^{-1} during the camera recording interval (Table 2). Similarly, during the 21 January 2020 event, wind speeds (U_{10}) were of comparable magnitude, with a daily average of 12.3 m s^{-1}, peak values reaching 13.2 m s^{-1} and values of about 12.5 m s^{-1} during the analysed

Table 2
Wind parameters (wind speed, U_{10}; wind direction, Dir_w) for the two analysed storm events (29 October 2018 and 21 January 2020), including daily average values, daily peak values and values corresponding to the camera recording interval.

Wind parameter	29 October 2018			21 January 2020		
	Daily average value	Daily peak value	Value during camera interval	Daily average value	Daily peak value	Value during camera interval
U_{10} (m s^{-1})	12.0	15.2	14.0	12.3	13.2	12.5
Dir_w (°)	211	231	241	113	114	114

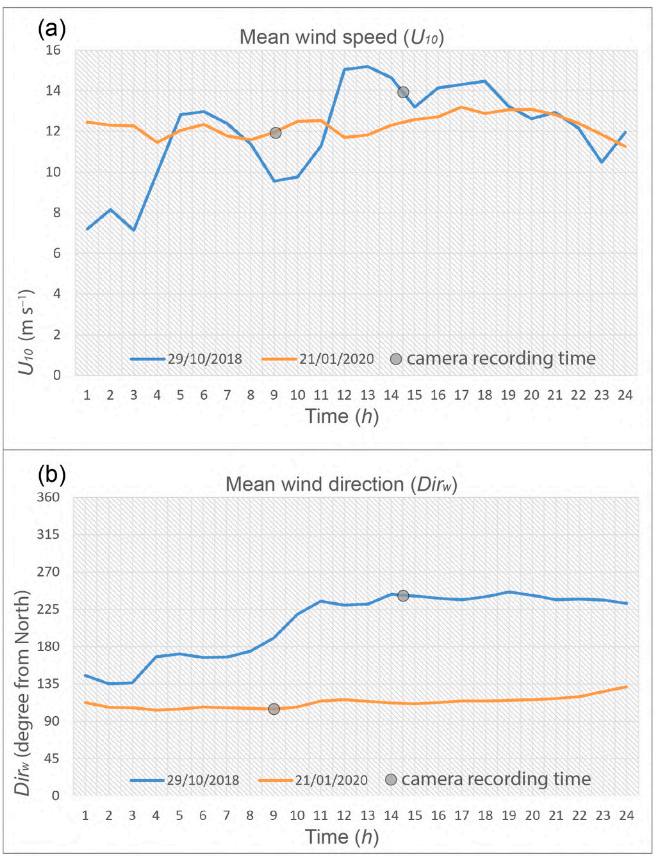

Fig. 5. Wind conditions derived from the ERA5 dataset during the two analysed storm events (29 October 2018 and 21 January 2020): **(a)** wind speed (U_{10}) and **(b)** wind direction (Dir_w). The grey dot indicates the wind conditions corresponding to the camera recording interval.

interval (Table 2). Despite the similar wind speeds, the two events were characterised by different wind directions (Table 2; Fig. 5). During the 2018 storm event, winds predominantly blew from the south-western sector, with mean directions ranging between 211° and 241°. In contrast, during the 2020 event winds mainly came from the east-south-eastern sector, with mean directions around 113-114° during the analysed period.

The application of the Peak Over Threshold (POT) approach allowed the identification of the temporal extent of the two storm events. The October 2018 event lasted 22 h, while the January 2020 event was longer, with a duration of 76 h. The total storm wave energy (E^i_{tot}) further highlights differences in storm intensity, with higher values recorded for the January 2020 event (1261.13 kWh m^{-1}) compared to the October 2018 event (479.64 kWh m^{-1}) (Table 3).

In the days following the 21 January 2020 storm event, wind conditions progressively shifted towards offshore directions (approximately 315°) and increased in intensity, with mean wind speeds of about 9.2 m s^{-1} and peak values of 13.4 m s^{-1} recorded between 4 and 5 February 2020 (Fig. 6).

4.2. Image analysis and swash dynamics

The analysis of georeferenced snapshots and DGPS-RTK beach profiles acquired prior to each storm event revealed substantial differences in the pre-storm backshore configuration despite the comparable offshore significant wave heights and wave periods described above.

The DGPS-RTK profiles (Fig. 7b) show that, prior to the 29 October 2018 storm event, the backshore was characterised by the absence of significant beach wrack accumulations due to previous beach-cleaning activities. The beach profile exhibited a foreshore slope (tan β_f) of 0.0633 and a berm crest elevation of 1.587 m above mean sea level (Fig. 7b).

In contrast, prior to the 21 January 2020 storm event, extensive beach wrack accumulations, mainly composed of *Arundo donax* reeds and *Posidonia oceanica* remains, formed a continuous ridge parallel to the shoreline, with the two components strongly intertwined (Fig. 2). These deposits contributed to a distinct backshore configuration, characterised by a steeper foreshore slope (tan $\beta_f = 0.1456$) and a berm crest elevation of 1.443 m above mean sea level (Fig. 7d). Although lower than the berm crest observed in 2018, the wrack ridge was located approximately 10 m seaward, increasing the foreshore slope (Fig. 7).

Infiltration measurements conducted along a nearby transect revealed substantial differences in the hydraulic properties of the investigated beach environments (Table 4). Permeability coefficients ranged from 6.67 × 10^{-5} m s^{-1} on the backshore sandy deposits to 3.3 × 10^{-4} m s^{-1} within the mixed beach wrack deposit composed of

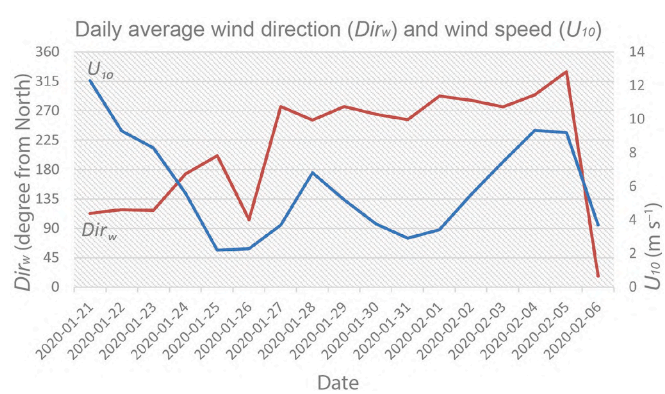

Fig. 6. Daily average wind speed (U_{10}) and wind direction (Dir_w) from the 21 January 2020 storm event to 5 February 2020 derived from the ERA5 reanalysis dataset. The figure highlights the development of offshore wind conditions in the days following the storm event.

Table 3
Temporal characteristics and total storm wave energy (E^i_{tot}) of the two analysed storm events.

Event	Storm start	Storm end	Peak intensity	Duration	E^i_{tot}
Oct 2018	29 Oct 2018 – 5:00	30 Oct 2018 – 02:00	29 Oct 2018 – 9:00	22 h	479.64 kWh m^{-1}
Jan 2020	20 Jan 2020 – 9:00	23 Jan 2020 – 12:00	21 Jan 2020 – 23:00	76 h	1261.13 kWh m^{-1}

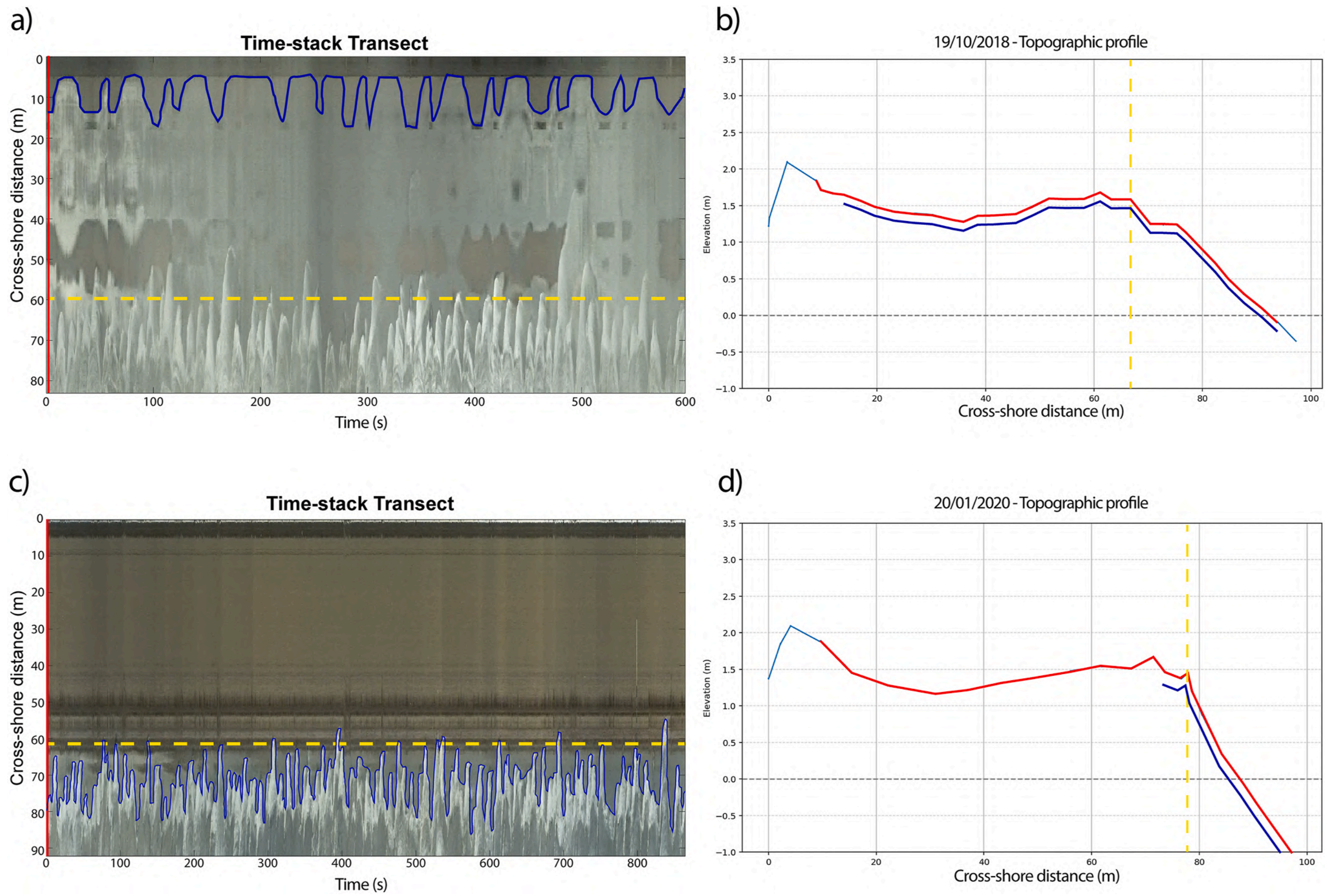

Fig. 7. Georeferenced time-stack images and corresponding DGPS-RTK beach profiles for the two analysed storm events: **(a, b)** 29 October 2018; **(c, d)** 21 January 2020. The time-stack images were extracted along the cross-shore transect shown in Fig. 2. Yellow dashed lines indicate the pre-storm berm crest derived from the DGPS-RTK surveys, while red lines mark the analysed cross-shore transect. Blue lines in the time-stack images represent the manually digitised swash fronts during the analysed recording intervals. In the corresponding beach profiles, the blue lines indicate the maximum landward extent of wave uprush derived from the digitised swash fronts. (For interpretation of the references to colour in this figure legend, the reader is referred to the Web version of this article.)

Table 4
Location, elevation, dominant material and permeability coefficients measured at different sectors of Poetto Beach using infiltration tests. Measurements were performed with double-ring infiltrometers following ASTM D3385, except for the *Posidonia oceanica* banquette, where a simplified single-ring infiltrometer was used because of the exceptionally high infiltration capacity of the seagrass deposits. A subset of these measurements was previously reported by Ruju et al. (2022). Coordinates are reported in the WGS84/UTM Zone 32N reference system.

Location	Latitude	Longitude	Elevation (m)	Dominant material	Permeability coefficient (m s^{-1})
Upper backshore	4339350.584473	514108.327681	1.1598	Sand	6.67×10^{-5}
Lower backshore	4339340.511586	514123.773709	1.3066	Sand	3.33×10^{-5}
Intertwined beach wrack deposit	4339332.106836	514139.695103	1.6600	Buried *Arundo donax* reeds and *Posidonia oceanica* remains	3.33×10^{-4}
Swash zone	4339330.213572	514144.392967	1.1101	Sand	2.33×10^{-4}
P. oceanica banquette	4339347.655449	514160.790053	0.8386	Banquette	from 1.14×10^{-1} to 1.50×10^{-1}

buried *Arundo donax* reeds and *Posidonia oceanica* remains. Intermediate values of approximately 2.3×10^{-4} m s^{-1} were measured in the swash zone.

In contrast, substantially higher infiltration rates, ranging from 1.14×10^{-1} to 1.50×10^{-1} m s^{-1}, were measured in four replicate tests on a nearby *Posidonia oceanica* banquette. These results indicate that mixed wrack deposits and classical *Posidonia oceanica* banquettes exhibit markedly different hydraulic properties and should not be considered equivalent (Table 4).

Time-stack analysis revealed that the 29 October 2018 storm event was characterised by repeated berm overtopping along the entire analysed transect, resulting in temporary backshore inundation extending approximately 50 m landward from the berm crest (Fig. 7a). In contrast, no berm overtopping was observed during the 21 January 2020 storm event within the analysed recording interval. Only a few wave uprush events partially exceeded the seaward edge of the sandy berm reinforced by a mixed beach wrack deposit composed of intertwined *Arundo donax* reeds and *Posidonia oceanica* remains, while the backshore remained free from inundation during the camera recording interval (Fig. 7c and d).

To further quantify the observed differences in wave overtopping potential, Total Water Level (TWL) values were estimated for both storm events at the specific times corresponding to the coastal video monitoring acquisitions, by combining tide-gauge observations with wave runup calculations following Stockdon et al. The empirical TWL reached 1.62 m above mean sea level during the 29 October 2018 recording and 2.24 m during the 21 January 2020 recording.

The empirical TWL exceeded the surveyed berm crest elevation during both events, by approximately 0.03 m in 2018 and 0.80 m in 2020. Despite the higher TWL estimated for the January 2020 storm, no berm overtopping or temporary backshore inundation was observed during the analysed recording interval. In contrast, repeated berm overtopping and extensive temporary backshore inundation occurred during the October 2018 event, when the estimated TWL was lower. (Fig. 7).

4.3. Hydrodynamic circulation

Hydrodynamic numerical simulations, performed using the Delft3D FLOW + WAVE Models, allowed the reconstruction of nearshore depth-averaged current velocity patterns during the two storm events analysed (Fig. 8).

During the camera recording interval of the 2018 storm event, waves approached Poetto beach predominantly from the southern sector, with significant wave heights of approximately 2.5 m. Numerical simulations indicate the development of longshore currents flowing from west to east along the western and central sectors of the beach. These currents were locally interrupted by offshore-directed rip current systems within the surf zone (Fig. 8a and b).

During the 2020 storm event, waves approached the beach mainly from the south-eastern sector, with significant wave heights of about 2.8 m. The simulated circulation pattern was broadly similar to that observed during the 2018 event, with the development of longshore currents and multiple rip current systems along the western and central sectors of Poetto beach (Fig. 8c and d).

Overall, the numerical simulations indicate depth-averaged current velocities ranging between approximately 0.2 and 0.7 m s^{-1}. The highest current velocities were observed near the extremities of the beach, where bathymetric gradients and coastal morphology influence nearshore circulation patterns.

5. Discussion

The comparison between the two storm events highlights marked differences in backshore response. Although the two events were characterised by comparable peak offshore wave heights and wave periods, they differed in mean wave directions and storm duration. Moreover, storm energy, estimated following Molina et al. (2019), was higher during the January 2020 event. Although the empirical TWL estimate exceeded the berm crest elevation during both storm events (Table 5), with an exceedance of approximately 0.03 m in October 2018 and 0.80 m in January 2020, no berm overtopping or temporary backshore inundation was observed during the analysed recording interval in 2020. In contrast, repeated berm overtopping and temporary backshore inundation occurred during the 2018 event, despite the lower estimated TWL. These observations suggest that hydrodynamic forcing alone cannot fully explain the different coastal responses observed during the analysed recording interval. It should be noted, however, that the Total Water Level estimates were derived from the empirical formulation of Stockdon et al. and therefore should be interpreted as first-order estimates of potential wave runup rather than direct evidence of swash excursion or overtopping.

Moreover, it should also be considered that the berm crest elevations used for the TWL analysis were derived from pre-storm DGPS-RTK surveys (Fig. 7b–d). During the October 2018 event, the camera recording interval occurred after the storm peak (Tables 3 and 5), and the berm morphology may therefore have already been modified by wave action before the analysed interval. Consequently, the actual berm crest elevation during the camera recording may have been lower than that measured in the pre-storm survey, contributing to the apparent discrepancy between the limited estimated TWL exceedance and the observed repeated berm overtopping. In contrast, during the January

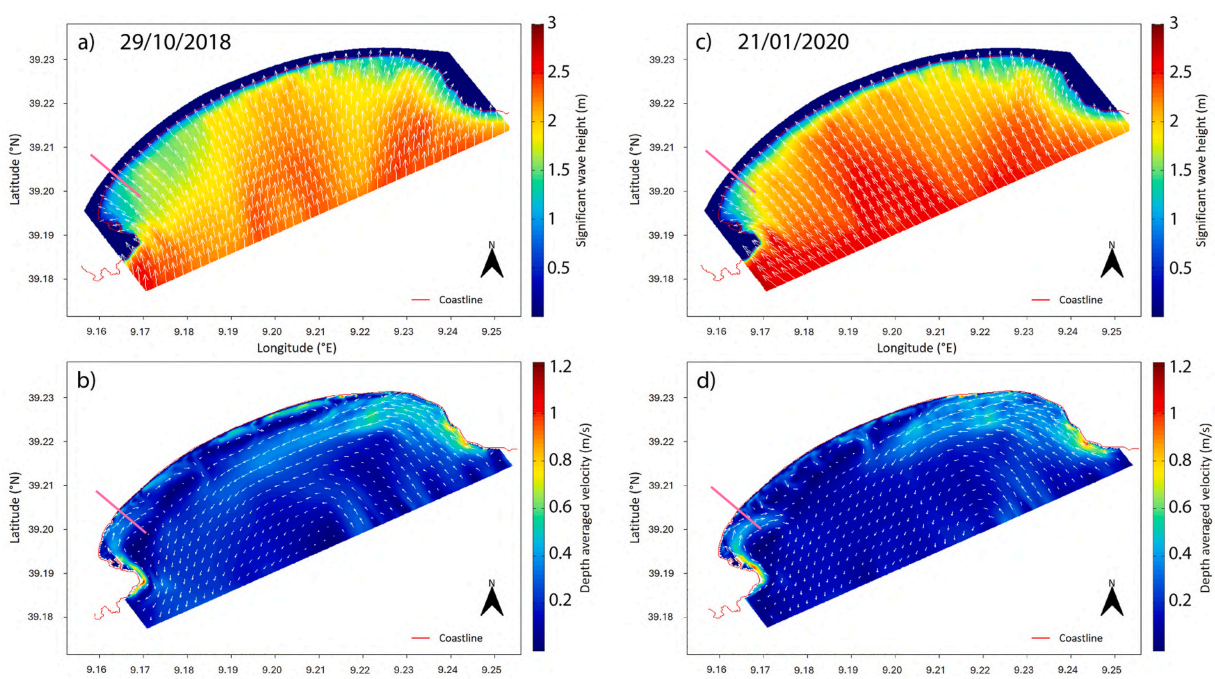

Fig. 8. Numerical simulation of wave and wind conditions during the two analysed storm events: **(a–b)** 29 October 2018; **(c–d)** 21 January 2020. The hydrodynamic conditions shown in all panels correspond to the time of the camera recording. Due to the different wave incidence, H_s values within the area covered by the camera were lower during the 2018 event compared to the 2020 event. Pink lines indicate the location of the analysed cross-shore transect. (For interpretation of the references to colour in this figure legend, the reader is referred to the Web version of this article.)

Table 5
Camera recording intervals, beach morphological parameters (berm crest elevation and foreshore slope), runup estimates ($R_{2\%}$), still water level $[Z_0(t) + T(t)]$, Total Water Level (TWL), and TWL exceedance relative to the berm crest for the analysed storm events.

Event	Camera recording interval (UTC)	Berm crest elevation (m.s.l.)	$\tan \beta_f$	$R_{2\%}$	$Z_0(t) + T(t)$	TWL	Exceedance
29/10/2018	14:00 - 14:10	1.587 m	0.0633	1.12 m	0.50 m	1.62 m	+ 0.03 m
21/01/2020	9:30 - 9:45	1.443 m	0.1455	2.09 m	0.15 m	2.24 m	+ 0.80 m

2020 event, the camera recording interval preceded the storm peak, which occurred later during the night (Tables 3 and 5), making the surveyed morphology more representative of the conditions during the analysed recording interval. As the storm peak occurred outside the daylight recording period, no video observations were available for that phase of the event.

Overall, the contrasting coastal response observed during the two storm events appears to result from the combined influence of hydrodynamic forcing and different backshore configurations, including the presence of a sandy berm reinforced by a mixed beach wrack deposit. During the October 2018 event, previous mechanical beach-cleaning operations had removed most of the beach wrack, leaving a relatively low and exposed sandy berm. Repeated use of heavy machinery may also have contributed to reducing the permeability of the sandy backshore. Prior to the January 2020 storm, a continuous mixed beach wrack deposit composed of intertwined *Arundo donax* reeds and *Posidonia oceanica* remains had developed approximately 10 m seaward of the 2018 berm crest, resulting in a steeper foreshore profile and a wider backshore. These geomorphological differences likely influenced the interaction between incoming waves and the backshore, limiting the landward propagation of wave uprush during the analysed recording interval. Similar effects have previously been reported for beach wrack and seagrass deposits, which may enhance wave energy dissipation and increase beach resilience during storm events (Kennedy and Woods, 2012; Ruju et al., 2022; Trogu et al., 2023).

The infiltration measurements further support this interpretation. The mixed beach wrack deposit composed of partially buried *Arundo donax* reeds and *Posidonia oceanica* remains exhibited a permeability coefficient of 3.33×10^{-4} m s^{-1}, approximately one order of magnitude higher than that measured on the sandy backshore (3.33×10^{-5} m s^{-1}). This increase suggests that the incorporation of vegetal material within the beach deposits enhances infiltration capacity and may promote the rapid drainage of overtopping water, thereby reducing the persistence of temporary backshore inundation (Ruju et al., 2022). Even higher permeability values (from 1.14×10^{-1} to 1.50×10^{-1} m s^{-1}) were measured on a nearby fresh *Posidonia oceanica* banquette, confirming the exceptionally high drainage capacity of unconsolidated seagrass accumulations reported in previous studies (Astudillo-Gutierrez et al., 2025).

It should be noted, however, that the two storm events differed not only in the presence of beach wrack but also in storm duration, wave and wind direction, and antecedent beach morphology. Consequently, the present observations should be interpreted as evidence from a comparative observational case study rather than as a controlled assessment of beach wrack effectiveness. The hydrodynamic modelling also has inherent uncertainties, as the simulations were not specifically validated against observations for the two analysed storm events and were intended to provide a broader representation of hydrodynamic circulation rather than a site-specific assessment of wave overtopping or beach-wrack effects. Overall, the combination of field observations, DGPS-RTK surveys, Total Water Level estimates, infiltration measurements and time-stack analysis suggests that differences in backshore morphologies due to the presence of the beach wrack may have contributed to the different beach responses observed during the recording intervals of the two events.

Field observations and imagery acquired before and after the January 2020 storm event further indicate that beach wrack accumulations are dynamic features that undergo significant redistribution during storm conditions. Prior to the storm, vegetal material was mainly organised in elongated longshore ridges (Fig. 9a). After the event, these deposits were partially reworked and redistributed along the backshore, forming cuspate sedimentary structures composed of coarse sediments intertwined with vegetal debris (Fig. 9c).

In the days following the January 2020 storm event, winds shifted offshore, with moderate intensities recorded during the camera observation intervals between 4 and 5 February 2020 (Fig. 6). Offshore winds are known to promote aeolian transport of sand across the backshore, enhancing sediment accumulation around surface roughness elements and obstacles (Bauer et al., 2009; McGuirk et al., 2022).

Imagery acquired from the coastal video monitoring system and field observations show that, during this post-storm phase, beach wrack deposits were progressively covered by wind-transported sand (Trogu et al., 2023) (Fig. 10).

The combined action of storm waves and subsequent aeolian processes therefore appears to control the morphodynamic evolution of beach wrack deposits. Storm waves redistribute and accumulate vegetal material along the backshore, while offshore winds promote sand trapping and the partial burial of these deposits within the beach sedimentary system (Trogu et al., 2023). When left undisturbed, these processes can persist over time, enhancing sediment accumulation and promoting backshore aggradation, as observed during the COVID-19 lockdown when the absence of beach-cleaning and other anthropogenic activities allowed beach wrack deposits to remain in place and favour continued aeolian sedimentation. The DGPS-RTK topographic profiles acquired in January and March 2020 (Fig. 11d) indicate that this process resulted in approximately 0.30 m of vertical accretion of the mixed beach wrack deposit composed of intertwined *Arundo donax* reeds and *Posidonia oceanica* remains.

Mediterranean beaches are characterised by marked seasonal storm activity, with the most energetic events generally occurring between autumn and spring (Androulidakis et al., 2015; Trogu et al., 2020; Flaounas et al., 2021). On urban beaches, these periods often coincide with continued recreational use, leading to frequent beach-cleaning operations and the mechanical removal of vegetal debris from both the beachface and the backshore (Simeone and De Falco, 2012; Boudouresque et al., 2016; Mossone et al., 2018; Astudillo-Gutierrez et al., 2025; Piscitelli et al., 2026).

Such operations, typically performed using heavy machinery, may compact beach sediments, reduce infiltration capacity and increase the persistence of overtopping water, thereby influencing the response of the backshore to storm-wave overtopping (Simeone and De Falco, 2012; Boudouresque et al., 2016; Ruju et al., 2022). The management of beach wrack along Mediterranean coasts is regulated by different frameworks that vary among countries. In Italy, national guidelines issued by the Ministry for the Environment provide the regulatory framework for the management of *Posidonia oceanica* beach wrack deposits (ISPRA, 2020). Although these regulations are primarily aimed at preventing coastal erosion and preserving environmental quality, they recognise that beach wrack removal may be appropriate under specific conditions. However, whenever compatible with local environmental and socio-economic requirements, management practices should also consider the potential influence of beach wrack removal on beach permeability and temporary storm-induced flooding, as summarised in Fig. 12.

The findings of this study highlight the potential role of adaptive beach wrack management as a Nature-Based Solution (NBS) for coastal protection, particularly in urban beach environments. The natural

Fig. 9. Beach wrack accumulations and sedimentary structures along the backshore of Poetto beach associated with the 21 January 2020 storm event: **(a)** accumulations of beach wrack (seagrass remains and river reeds) along the backshore before the storm event; **(c)** sedimentary structures observed along the backshore after the storm. Panels **(b)** and **(d)** indicate the locations of the camera views shown in panels **(a)** and **(c)**.

Fig. 10. Aeolian reworking of beach wrack deposits following the January 2020 storm event: **(a–b)** coastal video monitoring snapshots acquired on 4 and 5 February 2020, showing the progressive burial of beach wrack deposits due to wind-driven sand transport.

accumulation of beach wrack cannot, in and of itself, be considered a Nature-Based Solution. Instead, the potential NBS lies in management practices that preserve mixed wrack deposits *in situ* and minimise their removal, particularly through mechanical beach-cleaning operations. However, such natural sedimentary structures are not always present, as their formation and persistence also depend on local hydrodynamic and ecological conditions, including wave climate and seagrass supply (Trogu et al., 2023; Fernandez-Mora et al., 2025). By allowing storm-driven deposition and subsequent aeolian sediment trapping to proceed without disturbance, such management practices may enhance the natural processes that contribute to wave energy dissipation, sediment retention and backshore accretion, thereby increasing the resilience of Mediterranean beaches to storm impacts. Although the observations presented here support this management perspective, they should be interpreted as evidence from a two-event observational case study. Further investigations covering a larger number of storm events and different coastal settings are needed to evaluate the broader applicability and effectiveness of beach-wrack management as a Nature-Based Solution.

Overall, the observations presented in this study suggest that mixed beach wrack deposits may contribute to mitigating storm impacts by enhancing infiltration, promoting sediment retention and favouring backshore aggradation through the combined action of storm-wave deposition and subsequent aeolian sediment trapping.

From a coastal management perspective, these findings suggest that beach wrack should not be regarded solely as material to be routinely removed, even from urban beaches. Instead, management approaches that preserve mixed wrack deposits *in situ*, whenever compatible with local environmental, social and recreational requirements, may enhance the natural coastal protection services provided by beach wrack, including wave energy dissipation, sediment retention and backshore accretion, thereby increasing the resilience of Mediterranean beaches to storm impacts.

6. Conclusions

This study investigated the role of mixed beach wrack deposits in the storm response of an urban Mediterranean beach through the combined

Fig. 11. Detailed views of beach wrack deposits before and after aeolian sediment deposition: **(a)** 22 January 2020, showing the redistribution of beach wrack along the backshore after the storm event; **(b)** 28 March 2020, highlighting the burial of beach wrack deposits due to aeolian sand trapping. This process may contribute to beach accretion, thereby enhancing resilience to storm impacts. Panels **(c)** indicate the locations of the camera views shown in panels **(a)** and **(b)**. Panel **(d)** shows the comparison of the two topographic profiles, highlighting the accretion of the berm.

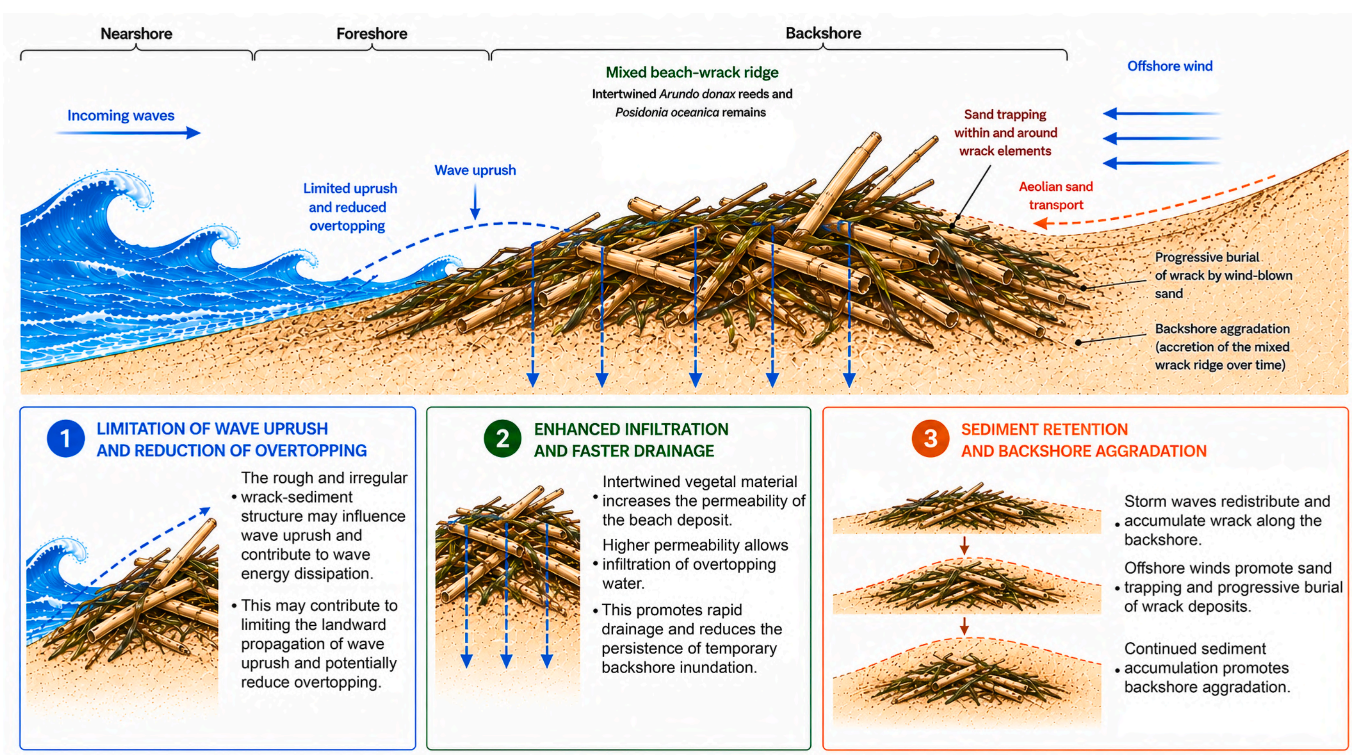

Fig. 12. Conceptual diagram illustrating the potential role of mixed beach-wrack deposits in modifying backshore response to storm conditions. The diagram summarises three interconnected processes: (1) potential limitation of wave uprush and potential reduction of berm overtopping due to the roughness and irregularity of the beach wrack; (2) enhanced infiltration and potentially faster drainage associated with the incorporation of vegetal material within the sandy beach body; and (3) sediment retention through aeolian sand trapping, progressive burial of the wrack deposits, and subsequent backshore aggradation.

analysis of coastal video monitoring, DGPS-RTK topographic surveys, infiltration measurements, Total Water Level estimates, storm-wave energy analysis and hydrodynamic modelling.

The comparison between the October 2018 and January 2020 storm events highlighted contrasting backshore responses during the analysed recording intervals, although the January 2020 event was characterised by higher storm-wave energy and a higher empirically estimated Total Water Level. During the 2020 analysed recording interval, no berm overtopping or temporary backshore inundation was observed at the monitored site, where the sandy berm was reinforced by a continuous beach wrack deposit composed of intertwined *Arundo donax* reeds and *Posidonia oceanica* remains. In contrast, repeated berm overtopping and temporary backshore inundation occurred during the 2018 event, when beach wrack had previously been removed through mechanical beach-cleaning operations. The observations suggest that the combined influence of hydrodynamic forcing, antecedent beach morphology and the presence of intertwined mixed beach wrack deposits may have contributed to these contrasting backshore responses.

The infiltration measurements indicate that the incorporation of vegetal material within the beach deposits increased infiltration capacity compared with the sandy backshore. In addition, successive DGPS-RTK surveys documented approximately 0.30 m of vertical accretion of the intertwined beach wrack deposit, reflecting the combined effects of storm-wave redistribution and subsequent aeolian sediment trapping.

Although the results should be interpreted as evidence from a comparative two-event observational case study, they support the view that adaptive beach wrack management, rather than the natural presence of beach wrack itself, may represent a promising Nature-Based Solution for Mediterranean beaches. Management approaches that preserve mixed wrack deposits *in situ*, whenever compatible with local environmental, social and recreational requirements, may enhance the natural coastal protection services provided by these deposits while maintaining the ecological functioning of the beach system. Further investigations covering a larger number of storm events and different coastal settings are needed to evaluate the broader applicability of these management strategies.

CRediT authorship contribution statement

Daniele Trogu: Writing – review & editing, Writing – original draft, Methodology, Formal analysis, Data curation, Conceptualization. **Antonio Usai:** Writing – review & editing, Methodology, Formal analysis, Data curation, Conceptualization. **Simone Simeone:** Writing – review & editing, Supervision, Methodology, Formal analysis, Data curation. **Marco Porta:** Writing – review & editing, Formal analysis, Data curation. **Sandro Demuro:** Writing – review & editing, Supervision, Project administration, Funding acquisition.

Declaration of generative AI and AI-assisted technologies in the manuscript preparation process

During the preparation of this work the author(s) used ChatGPT (OpenAI) in order to support language revision and improve the clarity of the manuscript. After using this tool/service, the author(s) reviewed and edited the content as needed and take(s) full responsibility for the content of the published article.

Declaration of competing interest

The authors declare that they have no known competing financial interests or personal relationships that could have appeared to influence the work reported in this paper.

Acknowledgements

This study was carried out within the RETURN Extended Partnership and received funding from the European Union Next-GenerationEU (National Recovery and Resilience Plan – NRRP, Mission 4, Component 2, Investment 1.3 – D.D. 1243 2/8/2022, PE0000005).

This publication was produced while attending the PhD programme in INNOVATION SCIENCES AND TECHNOLOGIES at the University of Cagliari, Cycle XXXVIII, with the support of a scholarship financed by the Ministerial Decree no. 351 of 9th April 2022, based on the NRRP - funded by the European Union - NextGenerationEU - Mission 4 "Education and Research", Component 1 ″Enhancement of the offer of educational services: from nurseries to universities'' - Investment 3.4 "Advanced teaching and university skills".

The research has also been funded by Regione Autonoma Sardegna (L.R. 7/2007) through the BEACH and TENDER NEPTUNE projects, directed by Sandro Demuro, University of Cagliari.

The authors thank Dr. Angelo Ibba for his contribution to this study and acknowledge the Sardinia Sea Port Authority, the Navy PolNato Depot of Cape S. Elia, MARICAGLIARI, and the Municipality of Cagliari for supporting the field activities. This study was carried out using E.U. Copernicus Marine Service information.

Appendix A. Supplementary data

Supplementary data to this article can be found online at https://doi.org/10.1016/j.ecss.2026.110253.

Data availability

Data will be made available on request.

References

Airy, G.B., 1845. Figure of the Earth, 5. Encyclopaedia Metropolitana, London, pp. 165–240.

Androulidakis, Y.S., Kombiadou, K.D., Makris, C.V., Baltikas, V.N., Krestenitis, Y.N., 2015. Storm surges in the Mediterranean Sea: variability and trends under future climatic conditions. Dynam. Atmos. Oceans 71, 56–82. https://doi.org/10.1016/j.dynatmoce.2015.06.001.

Armaroli, C., Duo, E., 2018. Validation of the coastal storm risk assessment framework along the Emilia-Romagna coast. Coast. Eng. 134, 159–167. https://doi.org/10.1016/j.coastaleng.2017.08.014.

Astudillo-Gutierrez, C., Pavo-Fernandez, E., Gracia, V., Sierra, J.P., Llull, T., Mosso, C., Sanchez-Artus, X., Sanchez-Arcilla, A., 2025. *Posidonia oceanica* banquette accumulations in southern Catalonia: management approaches and key parameters for coastal protection. Front. Mar. Sci. 12, 1681826. https://doi.org/10.3389/fmars.2025.1681826.

Barragán, J.M., De Andrés, M., 2015. Analysis and trends of the world's coastal cities and agglomerations. Ocean Coast Manag. 114, 11–20. https://doi.org/10.1016/j.ocecoaman.2015.06.004.

Bauer, B.O., Davidson-Arnott, R.G.D., Hesp, P.A., Namikas, S.L., Ollerhead, J., Walker, I. J., 2009. Aeolian sediment transport on a beach: surface moisture, wind fetch, and mean transport. Geomorphology 105, 106–116. https://doi.org/10.1016/j.geomorph.2008.02.016.

Biondo, M., Buosi, C., Trogu, D., Mansfield, H., Vacchi, M., Ibba, A., Porta, M., Ruju, A., De Muro, S., 2020. Natural vs. anthropic influence on the multidecadal shoreline changes of Mediterranean urban beaches: lessons from the Gulf of Cagliari (Sardinia). Water 12 (12), 3578. https://doi.org/10.3390/w12123578.

Booij, N., Ris, R.C., Holthuijsen, L.H., 1999. A third-generation wave model for coastal regions: 1. Model description and validation. J. Geophys. Res. Oceans 104 (C4), 7649–7666. https://doi.org/10.1029/98JC02622.

Borum, J., Duarte, C.M., Krause-Jensen, D., Greve, T.M., 2004. European seagrasses: an introduction to monitoring and management. *Monitoring and Managing of European Seagrasses Project* (M&MS), p. 88.

Boudouresque, C.F., Pergent, G., Pergent-Martini, C., Ruitton, S., Thibaut, T., Verlaque, M., 2016. The necromass of the *Posidonia oceanica* seagrass meadow: fate, role, ecosystem services and vulnerability. Hydrobiologia 781, 25–42. https://doi.org/10.1007/s10750-015-2333-y.

Brambilla, W., Van Rooijen, A., Simeone, S., Ibba, A., De Muro, S., 2016. Field observations, video monitoring and numerical modeling at Poetto Beach, Italy. J. Coast Res. 75, 825–829. https://doi.org/10.2112/SI75-166.1.

Chatzipavlis, A., Trogu, D., Ruju, A., Montes, J., Usai, A., Porta, M., Coco, G., De Muro, S., Ciavola, P., 2026. Development and validation of an Early Warning System for coastal flooding operating on a Mediterranean urban beach. NHESS 26, 1573–1601. https://doi.org/10.5194/nhess-26-1573-2026.

De Muro, S., Ibba, A., Simeone, S., Buosi, C., Brambilla, W., 2017. An integrated sea-land approach for mapping geomorphological and sedimentological features in an urban microtidal wave-dominated beach: a case study from S Sardinia, western Mediterranean. J. Maps 13 (2), 822–835. https://doi.org/10.1080/17445647.2017.1389309.

Duarte, C.M., 2002. The future of seagrass meadows. Environ. Conserv. 29 (2), 192–206. https://doi.org/10.1017/S0376892902000127.

EMODnet Bathymetry Consortium, 2024. EMODnet Digital Bathymetry (DTM 2024). Available online. https://doi.org/10.12770/cf51df64-56f9-4a99-b1aa-36b8d7b743a1. Last accesses in December 2025.

European Commission, 2015. Towards an EU Research and Innovation Policy Agenda for Nature-based Solutions & re-naturing Cities: Final Report of the Horizon 2020 Expert Group on 'Nature-based Solutions and Re-naturing Cities' - (Full Version). Publications Office. Available online: https://data.europa.eu/doi/10.2777/765301.

Fernandez-Mora, A., Gomez-Pujol, L., Coco, G., Orfila, A., 2025. Hydrodynamic conditions of Posidonia oceanica seagrass berm formation and dismantling events. Sci. Total Environ. 958, 178005. https://doi.org/10.1016/j.scitotenv.2024.178005.

Flaounas, E., Gray, S.L., Teubler, F., 2021. A process-based anatomy of Mediterranean cyclones: from baroclinic lows to tropical-like systems. Weather Clim. Dyn. 2, 255–279. https://doi.org/10.5194/wcd-2-255-2021.

Gobert, S., Cambridge, M., Velimirov, B., Pergent, G., Lepoint, G., Bouquegneau, J.-M., Dauby, P., Pergent-Martini, C., Walker, D., Larkum, A., Orth, R., Duarte, C., 2006. Biology of Posidonia. In: Seagrasses: Biology, Ecology and Conservation, pp. 387–408. https://doi.org/10.1007/1-4020-2983-7_17.

Gómez-Pujol, L., Orfila, A., Álvarez-Ellacuría, A., Terrados, J., Tintoré, J., 2013. *Posidonia oceanica* beach-cast litter in Mediterranean beaches: a coastal videomonitoring study. J. Coast Res. 165 (1), 1768–1773. https://doi.org/10.2112/SI65-299.

Hersbach, H., Bell, B., Berrisford, P., Biavati, G., Horányi, A., Muñoz Sabater, J., Nicolas, J., Peubey, C., Radu, R., Rozum, I., Schepers, D., Simmons, A., Soci, C., Dee, D., Thépaut, J.-N., 2023. ERA5 hourly data on single levels from 1940 to present. Copernicus Climate Change Service (C3S) Climate Data Store (CDS). https://doi.org/10.24381/cds.adbb2d47. Last accesses in November 2025.

Holthuijsen, L.H., 2007. Waves in Oceanic and Coastal Waters. Cambridge University Press.

IPCC, 2023. Climate Change 2021 - the Physical Science Basis: Contribution of Working Group I to the Sixth Assessment Report of the Intergovernmental Panel on Climate Change. Cambridge University Press, Cambridge, UK. https://doi.org/10.1017/9781009157896.

ISPRA, 2020. La Spiaggia Ecologica: Gestione Sostenibile Della Banquette Di *Posidonia Oceanica* Sugli Arenili Del Lazio. Manuali e linee guida ISPRA, Roma.

ISPRA: Tide Gauge Network – Cagliari Monitoring Station. Istituto Superiore per la Protezione e la Ricerca Ambientale. Available online: https://www.mareografico.it/it/stazioni.html. (Accessed 17 June 2026).

Kennedy, D.M., Woods, J.L.D., 2012. The influence of coarse woody debris on gravel beach geomorphology. Geomorphology 159–160, 106–115. https://doi.org/10.1016/j.geomorph.2012.03.009.

Komar, P.D., 1998. In: Beach Processes and Sedimentation, second ed. Prentice Hall, Englewood-Cliffs.

Korres, G., Ravdas, M., Denaxa, D., Sotiropoulou, M., 2021. Mediterranean Sea Waves Reanalysis INTERIM (CMEMS Med-Waves, MedWAM3I system) (Version 1). Data set Copernicus Monitoring Environment Marine Service (CMEMS). https://doi.org/10.25423/CMCC/MEDSEA_MULTIYEAR_WAV_006_012_MEDWAM3I. Last accesses in November 2025.

Lesser, G.R., Roelvink, J.A., van Kester, J.A.T.M., Stelling, G.S., 2004. Development and validation of a three-dimensional morphological model. Coast. Eng. 51 (8–9), 883–915. https://doi.org/10.1016/j.coastaleng.2004.07.014.

Manfra, L., Chiesa, S., Simeone, S., Borrello, P., Piermarini, R., Agaoglou, C., Elbour, M., Zaaboub, N., Vandarakis, D., Kourliaftis, I., Scarpato, A., Rotini, A., 2024. Towards sustainable management of beach-cast seagrass in Mediterranean coastal areas. Sustainability 16 (2), 756. https://doi.org/10.3390/su16020756.

Mateo, M.-Á., Sánchez-Lizaso, J.-L., Romero, J., 2003. Posidonia oceanica 'banquettes': a preliminary assessment of the relevance for meadow carbon and nutrients budget. Estuar. Coast Shelf Sci. 56, 85–90. https://doi.org/10.1016/S0272-7714(02)00123-3.

Mathiesen, M., Goda, Y., Hawkes, P.J., Mansard, E., Martín, M.J., Peltier, E., Thompson, E.F., Van Vledder, G., 1994. Recommended practice for extreme wave analysis. J. Hydraul. Res. 32 (6), 803–814. https://doi.org/10.1080/00221689409498691.

McGuirk, M.T., Kennedy, D.M., Konlechner, T., 2022. The role of vegetation in incipient dune and foredune development and morphology: a review. J. Coast Res. 38, 414–428. https://doi.org/10.2112/JCOASTRES-D-21-00021.1.

Molina, R., Manno, G., Lo Re, C., Anfuso, G., Ciraolo, G., 2019. Storm energy flux characterization along the mediterranean Coast of Andalusia (Spain). Water 11, 509. https://doi.org/10.3390/w11030509.

Mossone, P., Guala, I., Heurtefeux, H., Giunta Fornasin, M.E., Issaris, Y., Gerakaris, V., Salomidi, M., Milano, P., Guido, M., Marciano, V., Otero, M.M., Aljinovic, B., Simeone, S., 2018. POSBEMED: Posidonia beach/dunes socio-economic Evaluation, 2. Final Report, Technical report. IMC Foundation - International Marine Centre, 70pp.

Narayan, S., Beck, M.W., Reguero, B.G., Losada, I.J., van Wesenbeeck, B., Pontee, N., Sanchirico, J.N., Ingram, J.C., Lange, G.M., Burks-Copes, K.A., 2016. The effectiveness, costs and coastal protection benefits of natural and nature-based defences. PLoS One 11 (5), e0154735. https://doi.org/10.1371/journal.pone.0154735.

Neumann, B., Vafeidis, A., Zimmermann, J., Nicholls, R., 2015. Future coastal population growth and exposure to sea-level rise and coastal flooding - a global assessment. PLoS One 10 (6), e0131375. https://doi.org/10.1371/journal.pone.0118571.

Nicholls, R.J., Cazenave, A., 2010. Sea-level rise and its impact on coastal zones. Science 328, 1517–1520. https://doi.org/10.1126/science.1185782.

Ondiviela, B., Losada, I.J., Lara, J.L., Maza, M., Galván, C., Bouma, T.J., Van Belzen, J., 2014. The role of seagrasses in coastal protection in a changing climate. Coast. Eng. 87, 158–168. https://doi.org/10.1016/j.coastaleng.2013.11.005.

Passarella, M., 2019. On the Prediction of Swash Excursion and the Role of Seagrass beach-cast Litter: Modelling and Observations. University of Cagliari, Cagliari, Italy. PhD Thesis.

Patra, A., Oueslati, B., Chevallier, T., Renaud, P., Kervella, Y., Dubus, L., 2025. Evaluation of ERA5, COSMO-REA6 and CERRA in simulating wind speed along the French coastline for wind energy applications. Adv. Sci. Res. 22, 69–85. https://doi.org/10.2139/ssrn.5131628.

Pikelj, K., Godec, P., Tesovic, B.C., 2022. Sedimentological Consequences of *Posidonia oceanica* Banquette Removal: Sakarun Beach Case Study (Dugi Otok, Croatia). Firenze University Press. https://doi.org/10.36253/979-12-215-0030-1.08.

Piscitelli, E., Manfra, L., Pettini, G., Matano, F., Vicinanza, D., Rotini, A., 2026. A georeferenced dataset of *Posidonia oceanica* deposits and banquettes for mapping and coastal management along Mediterranean seashores. Discov. Geosci 4, 97. https://doi.org/10.1007/s44288-026-00444-2.

Porta, M., Buosi, C., Trogu, D., Ibba, A., De Muro, S., 2020. An integrated sea-land approach for analyzing forms, processes, deposits and the evolution of the urban coastal belt of Cagliari. J. Maps 17, 65–74. https://doi.org/10.1080/17445647.2020.1719441.

Pugh, D.T., 1987. Tides, Surges, and Mean Sea-Level: a Handbook for Engineers and Scientists. John Wiley and Sons Ltd., Hoboken, New York, USA, p. 472.

Ris, R.C., Holthuijsen, L.H., Booij, N., 1999. A third-generation wave model for coastal regions: 2. Verification. J. Geophys. Res. 104 (C4), 7667–7681. https://doi.org/10.1029/1998JC900123.

Rotini, A., Chiesa, S., Manfra, L., Borrello, P., Piermarini, R., Silvestri, C., Cappucci, S., Parlagreco, L., Devoti, S., Pisapia, M., Creo, C., Mezzetti, T., Scarpato, A., Migliore, L., 2020. Effectiveness of the "Ecological Beach" Model: Beneficial Management of posidonia beach casts and banquette. Water 12. https://doi.org/10.3390/w12113238.

Ruju, A., Buosi, C., Coco, G., Porta, M., Trogu, D., Ibba, A., De Muro, S., 2022. Ecosystem services of reed and seagrass debris on a urban Mediterranean beach (Poetto, Italy). Estuar. Coast Shelf Sci. 271, 107862. https://doi.org/10.1016/j.ecss.2022.107862.

Ruju, A., Passarella, M., Trogu, D., Buosi, C., Ibba, A., De Muro, S., 2019. An operational wave system within the monitoring program of a mediterranean beach. J. Mar. Sci. Eng. 7, 32. https://doi.org/10.3390/jmse7020032.

Sardegna Geoportale, 2026. WMS – Regione Autonoma Della Sardegna. Available online: https://webgis.regione.sardegna.it/geoserverraster/ows?service=WMS&request=GetCapabilities. last accesses in January 2026.

Simeone, S., De Falco, G., 2012. Morphology and composition of beach-cast *Posidonia oceanica* litter on beaches with different exposures. Geomorphology 151–152, 224–233. https://doi.org/10.1016/j.geomorph.2012.02.005.

Small, C., Nicholls, R.J., 2003. A global analysis of human settlement in coastal zones. J. Coast Res. 19 (3), 584–599.

Stockdon, H.F., Holman, R.A., Howd, P.A., Sallenger, J.A.H.: Empirical parameterization of setup, swash, and runup. Coast. Eng. 53, 573–588, https://doi.org/10.1016/j.coastaleng.2005.12.005.

Telesca, L., Belluscio, A., Criscoli, A., Ardizzone, G., Apostolaki, E.T., Fraschetti, S., Gristina, M., Knittweis, L., Martin, C.S., Pergent, G., Alagna, A., Badalamenti, F., Garofalo, G., Gerakaris, V., Louise Pace, M., Pergent-Martini, C., Salomidi, M., 2015. Seagrass meadows (*Posidonia oceanica*) distribution and trajectories of change. Sci. Rep. 5, 12505. https://doi.org/10.1038/srep12505.

Temmerman, S., Meire, P., Bouma, T.J., Herman, P.M.J., Ysebaert, T., De Vriend, H.J., 2013. Ecosystem-based coastal defence in the face of global change. Nature 504, 79–83. https://doi.org/10.1038/nature12859.

Tomasello, A., Bosman, A., Signa, G., Rende, S.F., Andolina, C., Cilluffo, G., Cassetti, F.P., Mazzola, A., Calvo, S., Randazzo, G., Scarpato, A., Vizzini, S., 2022. 3D-reconstruction of a giant Posidonia oceanica beach wrack (Banquette): sizing biomass, carbon and nutrient stocks by combining field data with high-resolution UAV photogrammetry. Front. Mar. Sci. 9, 903138. https://doi.org/10.3389/fmars.2022.903138.

Trogu, D., Buosi, C., Ruju, A., Porta, M., Ibba, A., De Muro, S., 2020. What happens to a Mediterranean microtidal wave-dominated beach during significant storm events? The morphological response of a natural Sardinian Beach (Western Mediterranean). J. Coast Res. 95, 695. https://doi.org/10.2112/SI95-135.1.

Trogu, D., Simeone, S., Ruju, A., Porta, M., Ibba, A., DeMuro, S., 2023. A four-year video monitoring analysis of the *Posidonia oceanica* banquette dynamic: a case study from an urban microtidal Mediterranean beach (Poetto beach, Southern Sardinia, Italy). J. Mar. Sci. Eng. 11, 2376. https://doi.org/10.3390/jmse11122376.

Usai, A., Simeone, S., Trogu, D., Porta, M., Demuro, S., 2025a. A morphometric analysis of embayed beaches: southern Sardinia Island. Geomorphology 483, 109838. https://doi.org/10.1016/j.geomorph.2025.109838.

Usai, A., Trogu, D., Porta, M., Demuro, S., Simeone, S., 2025b. 70 years of shoreline changes in southern sardinia (Italy): Retreat and accretion on 79 mediterranean microtidal beaches. Water 17, 2517. https://doi.org/10.3390/w17172517.
Vacchi, M., De Falco, G., Simeone, S., Montefalcone, M., Morri, C., Ferrari, M., Bianchi, C.N., 2017. Biogeomorphology of the Mediterranean *Posidonia oceanica* seagrass meadows. Earth Surf. Process. Landf. 42, 42–54. https://doi.org/10.1002/esp.3932.
Vousdoukas, M.I., Ranasinghe, R., Mentaschi, L., Plomaritis, T.A., Athanasiou, P., Luijendijk, A., Feyen, L., 2020. Sandy coastlines under threat of erosion. Nat. Clim. Change 10, 260–263. https://doi.org/10.1038/s41558-020-0697-0.